Article

Assessment of Hydrological Processes in an Ungauged Catchment in Eritrea

Elisa Baioni [1],*, Giovanni Michele Porta [1], Nelly Cattaneo [2] and Guadagnini Alberto [1]

[1]   Department of Civil and Environmental Engineering, Politecnico di Milano, 20133 Milan, Italy;
       giovanni.porta@polimi.it (G.M.P.); alberto.guadagnini@polimi.it (G.A.)
[2]   Department of Architecture and Urban Studies, Politecnico di Milano, 20133 Milan, Italy;
       nelly.cattaneo@polimi.it
*   Correspondence: elisa.baioni@polimi.it

Abstract: This study investigates the surface processes taking place in an ungauged catchment in the Foro region in Eritrea (East Africa). We focus on estimating river discharge, sediment transport, and surface runoff to characterize hydrological fluxes in the area and provide a preliminary quantification of sediment transport and erosion. In this context, an overarching objective of the research is the study of the catchment associated with the Foro Dam. The latter comprises a silted reservoir formerly employed for agricultural water supply. The main traits associated with the system behavior across the watershed are assessed for a variety of combinations of the parameters governing the hydrological model selected. A detailed sensitivity analysis is performed to quantify the effects of the hydrological parameters on the estimated results. Numerical analyses are then performed to obtain an appraisal of expected water and sediment fluxes. Outputs of interest are largely dominated by the curve number parameter.

Keywords: water management; developing countries; streamflow modeling; erosion; sensitivity analysis; numerical modeling; cooperation projects

1. Introduction

Scarcity of freshwater resources is a major issue of concern worldwide. In Sub-Saharan Africa the situation is exacerbated by possible impacts associated with climate dynamics and the expected significant population growth. These elements pose special concerns in countries where economic and management issues might somehow challenge easy accessibility to fresh water [1,2]. The high temperatures recorded in recent years amplify water evaporation and population increase, enhancing water demands. Eritrea is tied to the third-highest urban population growth rate in Africa for the period 2000–2005 [3]. Hydrological models can then become useful tools for resources assessment and management, e.g., to quantify water volumes that can be considered to possibly meet the water demand.

This study is framed in the context of the VITAE project [4–6]. The latter is centered on the sustainable valorization of the Eritrean heritage Adulis archaeological site. It is an inter- and multi-disciplinary project geared towards designing and creating a sustainable archaeological park including a research center and a guest house nearby. From a water management perspective, the site is located close to the Foro Dam. The latter was formerly used for agricultural water supply, a service which is currently hampered due to excessive deposition of solid material. In this context, the work focuses on the investigation of the key surface processes (comprising the river discharge, sediment transport, and runoff) that take place in the Eritrean Foro region in the proximity of the Foro Dam. Water management has been recognized as a priority for the safeguard of the archaeological site of Adulis and to secure viable water supply for agriculture and domestic uses in the surrounding villages, alternately threatened by floods and drought.

Estimation of water fluxes is essential to identify the best intervention strategy. Available hydrological models (see, e.g., [7] and references therein) include (*a*) conceptual models, which describe hydrological processes through a set of differential equations based on a combination of simplified assumptions driving the hydraulic behavior of the system and embedded in empirical algebraic equations, and (*b*) differential models, which are based on conservation of mass, energy, and momentum. The former group includes, e.g., frameworks such as SSARR (Stream Synthesis and Reservoir Regulation Model) [8], the tank model [9], HEC-1 (Hydrologic Engineering Center) [10], and HYMO (Hydrologic Model) [11]. The latter set of models includes, e.g., the SHE (Systeme Hydrologique Europeen) model [12] or the IHDM (Institute of Hydrology Distributed Model) model [13]. Other modeling efforts have been proposed in the early 1980s to simulate the effects of land management on water and sediment transport, as well as nutrients dynamics. For instance, the CREAMS (Chemicals, Runoff and Erosion from Agriculture Management Systems) model developed by USDA (United States Department of Agriculture) [14] is structured across three separate components: (1) hydrology for the estimation of runoff, (2) erosion/sediment yield to quantify transport of sediments, and (3) chemistry to describe the movement of plant nutrients, pesticides, and other chemicals from distributed sources. The GLEAMS (Groundwater Loading Effects on Agricultural Management Systems) [15] and EPIC (Erosion-Productivity Impact Calculator) [16] models represent an evolution of the CREAMS model. The former simulates pesticide groundwater loading while the latter aims at assessing the impact of erosion on crops. The three hydrological models mentioned above (i.e., CREAMS, GLEAMS, EPIC) contributed significantly to the implementation of the modeling framework SWAT (soil and water assessment tool) developed by the USDA-Agricultural Research Service [17] to predict the influence of management on water, sediments, and agrochemicals in ungauged basins [7]. This modeling framework offers several advantages: (a)the use of readily available inputs for large areas; (b) a remarkable computational efficiency even when applied to large watersheds; (c) its ability to enable simulation of long time periods to evaluate the effects of changes in management strategies; (d) the use of a GIS interface for preprocessing of input data and visualization of modeling results; and (e) its suitability for application to ungauged basins where calibration of model parameters is challenging.

The hydrological analysis presented in this study is based on the framework provided by the SWAT suite. Moreover, SWAT has been already successfully applied in climatic and geographical contexts [2,18–21] similar to the setting here considered. Key objectives of the modeling effort include (i) estimation of the river discharge and sediment transport across the watershed and near Foro Dam and their interannual variability, and (ii) quantification of the variation in surface runoff throughout the entire hydrographic basin. Calibration and validation of the hydrological model in this context is challenging due to the paucity of observed data. The spatial pattern of the hydrologic variables across the catchment is evaluated under the default model parameterization and for various combinations of model parameters, in the context of a detailed sensitivity analysis. The latter enables us to quantify the impact of the uncertain hydrological parameters on river outflow rate, amount of sediment transported, and surface runoff.

The work is organized as follows: the region subject to our analysis is illustrated in Section 2, while the collection of input data required to initialize the hydrological model is presented in Section 3. Preprocessing of topographic data, soil properties, and land use information is tackled in Section 4. A brief description of the hydrological model used to simulate the main surface hydrological processes within the watershed is provided in Section 5. The numerical results are presented and discussed in Section 6, while key findings are summarized in the conclusion.

2. Study Site

The study is conducted in the catchment area including Foro Dam (see Figure 1). The latter is located 3 km upstream of the archaeological site of Adulis. The area lies within

a delta fan bounded by the isolated mountain of Ghedem to the Northwest, the eastern central highland slopes to the west, and the Red Sea to the east. The area is characterized by a marked alluvial activity. As reported by the Periplus of the Erythrean Sea (first c. A.D.), the city of Adulis, located a few kilometers from the dam, was a city and the hub of the Mediterranean–Indian Ocean trade [22]. Due to a remarkable localized environmental change and the ensuing deposition of a significant amount of alluvial sediments, Adulis is now 7 km from the coast.

The reference area is characterized by a semiarid climate. The hot season ranges from June to September with a temperature varying between 40–50 °C. The rainy season typically comprises the months from December to February (T = 20–35 °C), mild rains being generally observed in October and November. The average annual temperature is about 30 °C with an overall annual precipitation of about 200 mm.

The site is drained by the Haddas and Alighede rivers and numerous tributaries. These rivers form steep valleys that are typically narrow and winding. The Haddas River collects water from the Komayle and Alighede watercourses and is at the same time a resource and a vulnerability factor for the Zula, Afta, and Foro areas. These are subject to seasonal flooding, as evidenced by fluvial depositional layers observed during direct inspections along the western bank of the Haddas River [5,22]. Flooding events of the 7th–8th centuries AD likely caused the destruction of Adulis. In 1924, the floods of the Haddas river broke the soil and stone barrier built a few years earlier, causing severe destruction of downstream plantations, while in the winter of 2015 they damaged the village of Foro, leading to a reduction in agricultural and farming activities in the area [5]. Sudden and violent floods represent a serious risk for the preservation of the archaeological site.

The upstream areas around the areas of Foro and Ghedem mountain are characterized by conglomerates, vesicular basalt, and pyroclastic rocks, gneisses, and mica schist with mafic dykes [22]. As displayed in Figure 1, there is a natural rift near Foro dam. It is constituted by a break in the basaltic rock terrace of about 50 m width and 14 m height and is suitable to be potentially converted into a reservoir to supply water for agriculture and to contain floods. The existing dam was built in the late 1950s and was used as an infrastructure regulating water source for the terraced irrigation system in the coastal area. Since early 2000, it has been completely silted up due to sediment depositions caused by the channel erosion and lack of silt traps (check dams) [23]. The alluvial overburden comprises unconsolidated alluvial sediments transported from the central highland hills and Ghedem Mountain. Agriculture at the site relies on the spate irrigation consisting of a reservoir and a series of canals dug into the ground and connecting the reservoir to the fields. Seasonal water is collected by a barrier and is diverted through primary and secondary canals to the fields. These range in size from 1 to 3 ha and are surrounded by soil embankments up to 2 m high, the latter serving to store water and mitigate adverse flood effects. When water is insufficient, the secondary canals are closed and the fields further away from the reservoir are abandoned. In the present day, the inefficiency of the dam has decreased the amount of water available for agriculture. This has resulted in a reduction of the cultivated area from 10,000 to 1000 ha [5]. While restoring the dam would lead to a clear improvement of the possibility to irrigate crops, impacts of flood events and sediment transport require careful consideration of appropriate management strategies.
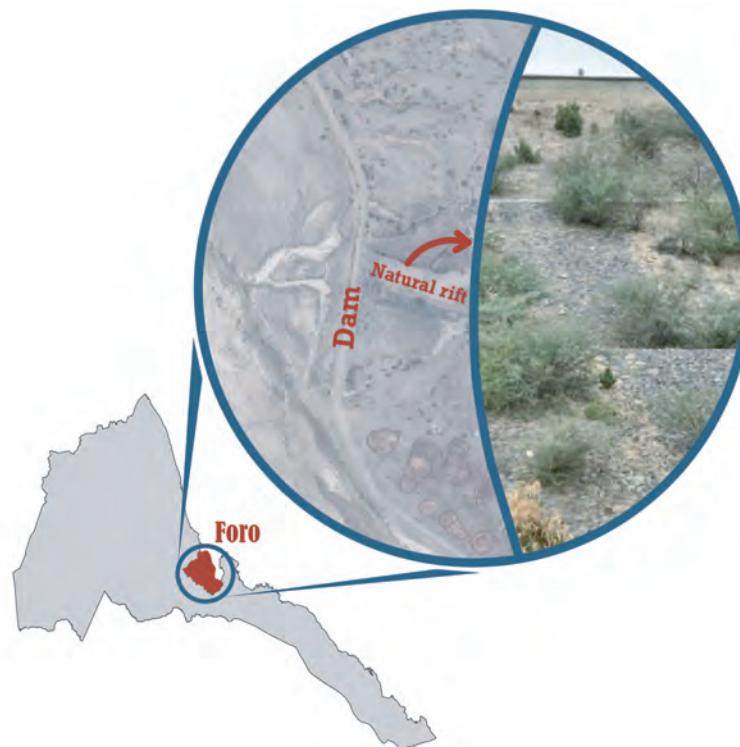
Figure 1. Study area: satellite view of the dam at Foro and the natural rift.

3. Data Collection

The procedure of building a hydrological model, such as the one considered here, is typically structured across four steps: (*i*) data collection, (*ii*) data preprocessing, (*iii*) simulation, and (*iv*) calibration and validation of results. Data collection considers (*a*) the topography of the area, (*b*) the land use, (*c*) the soil type, and (*d*) precipitation information. The source and the use of these data types are listed in Table 1.

Table 1. Data collection: DEM, land cover map, soil map, precipitation.

Data Type	Purpose	Provider	URL
DEM (digital elevation model)	Delineation of watershed of the area and stream network	NASA	https://search.earthdata.nasa.gov/, accessed on 15 May 2021
Land cover map	Identification of the land use for each HRU of the watershed	FAO	https://www.fao.org/3/x0596e/x0596e00.htm, accessed on 15 May 2021
Soil map	Identification of the soil type for the parameterization of infiltration, runoff and evapotranspiration fluxes	FAO	https://data.apps.fao.org/map/catalog/srv/ita/catalog.search#/metadata/ca4628f0-88fd-11da-a88f-000d939bc5d8, accessed on 15 May 2021
Climatic data	Daily data of precipitation, wind, relative humidity, and solar radiation	National Centers for Environmental Prediction (NCEP)	https://globalweather.tamu.edu/, accessed on 15 May 2021

Data preprocessing is performed in the Geographic Information System (GIS) environment upon relying on the QGIS platform and on algorithms implemented in the plugin QSWAT [24]. The latter tool allows delineating the watershed and hydrological response units (HRUs), which are then used as basic elements for the numerical simulations performed in SWAT [17]. As mentioned above, major quantities of interest in our study include (*a*) the daily river discharges and their interannual variability, (*b*) sediment transport, and (*c*) the quantification of the surface runoff across the whole catchment. At the current stage, the lack of available measured data prevents calibration and subsequent validation of the model. Hence, a rigorous sensitivity analysis is performed to evaluate the impact of uncertain model parameters on the target outputs. Doing so enables one to identify which parameters should be targeted in future field measurement campaigns.

SWAT requires specific information on topography, soil properties, land use, and weather of the catchment area to effectively model the physical processes associated with water movement and sediment transport. Details on the collected data are provided in the following sections.

3.1. Digital Elevation Model, Land Cover, and Soil Properties

A DEM with a resolution of 30 m × 30 m (see Figure 2) is provided by the NASA Shuttle Radar Topography Mission Global and is here used to obtain topographic information, including local elevation and slope, of the study area.
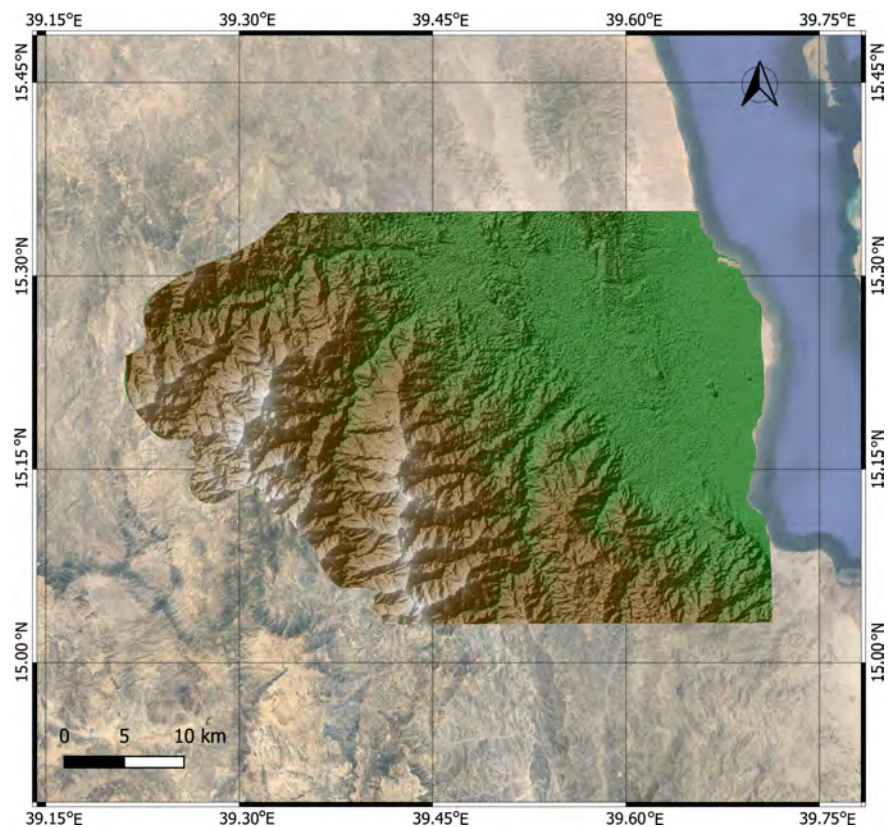

Figure 2. Digital elevation model of the study area.

The land use map depicted in Figure 3 is derived from the land cover map of Eritrea provided by the Food and Agriculture Organization (FAO) of the United Nations. The Land Cover Classification System (LCCS) is employed, distinguishing eight main categories. Land use classes are reclassified to match the land use code in SWAT. Details about the applied conversion from FAO to SWAT code classes are included in Table 2.

Table 2. Correspondence between FAO and SWAT land use categories.

Description FAO	Description SWAT	SWAT Code
Low sparse sHRUbs with herbaceous. SHRUbs density varies from 1 to 15%	Range grasses	RNGE
Very open sHRUbs with herbaceous from closed to open. The height of sHRUbs varies from 0.3 to 5 m. SHRUbs density varies from 40 to 65%	Range brush	RNGB
Needleleaved evergreen closed trees with sHRUbs	Forest evergreen	FRSE
Closed woody vegetation	Forest—mixed	FRST
Irrigated herbaceous crop, large to medium fields—cereal. Irrigated cereals crop. Fields density comprises from 20 to 49. Non-perennial river	Agriculture land—generic	AGRL
Sand	Rock sand	UIDU
Non-perennial river	Water	WATR
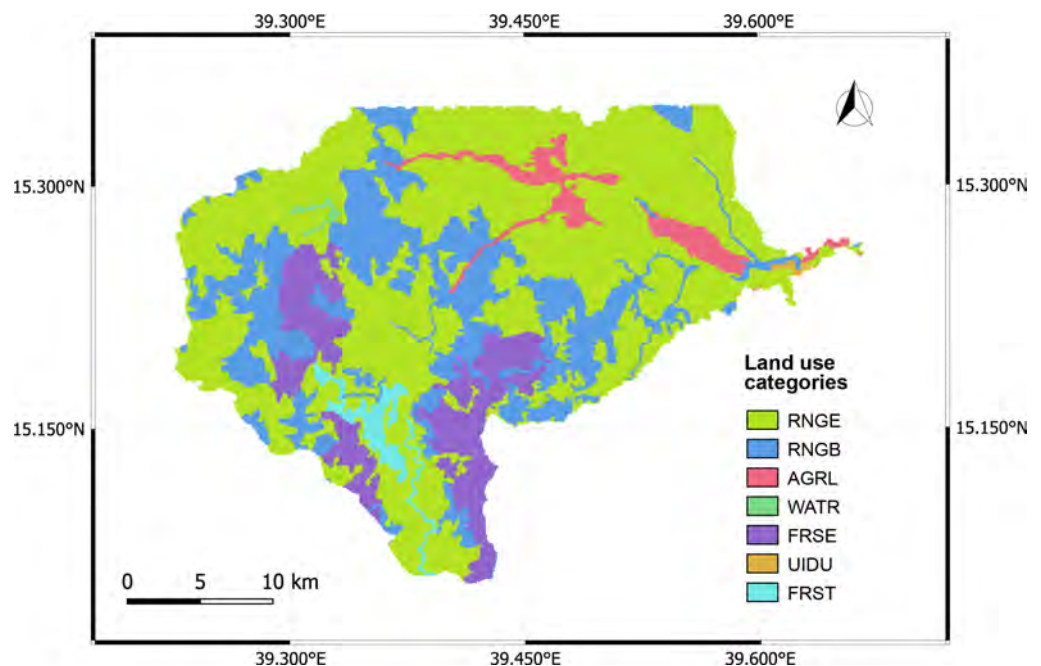
Figure 3. Land cover map: RNGE (range grasses), RNGB (range brush), AGRL (agriculture land—generic), WATR (water), FRSE (forest evergreen), UIDU (rock sand), FRST (forest—mixed). The description of the land cover categories is provided in Table 2.

For each soil category indicated in Figure 4, the clay, sand, and silt percentage is estimated by averaging the associated SoilGrids250m [25,26] data. These quantities are employed to identify the hydrological group. This information is in turn employed to obtain curve number estimates, upon considering the classical USDA soil texture triangle [27]. The soil texture and the corresponding hydrological soil group are listed in Table 3 for each soil category.
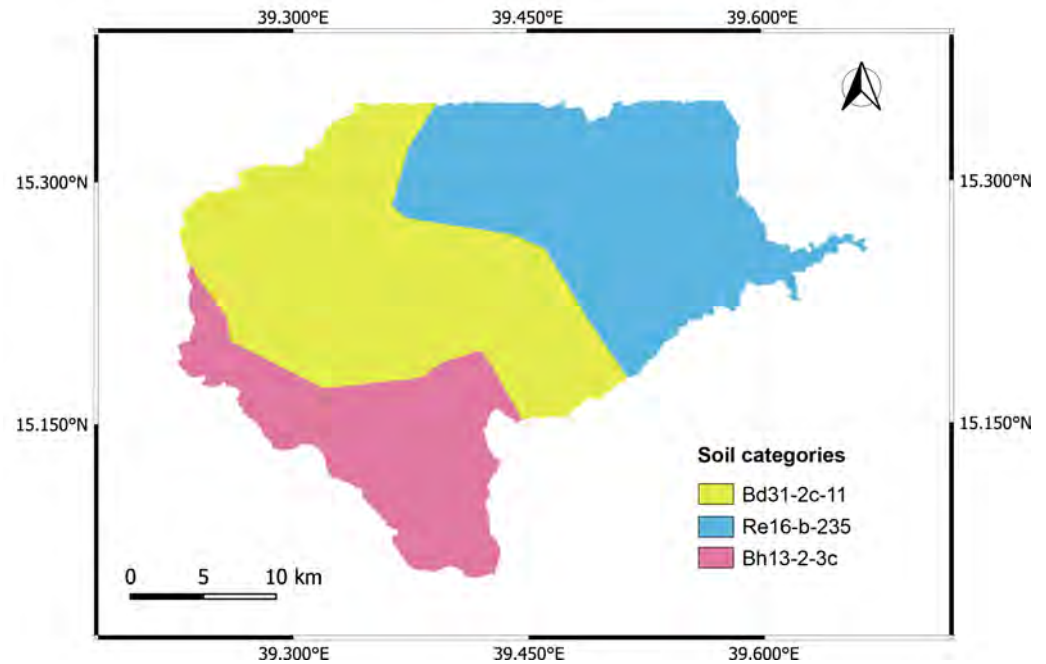
Figure 4. Soil map provided by FAO. The clay, sand, and silt content of each soil group determined by SoilGrids250m [25] data are listed in Table 3.

Table 3. Clay, sand, and silt content (%), textural class, and hydrological soil group for the soil categories Bd31-2c-11, Re16-b-235, Bh13-2-3c in Figure 4.

Code	Depth (cm)	Clay Content (%)	Sand Content (%)	Silt Content (%)	Textural Class	Hydrologic Soil Group
Bd31-2c-11	0-5	27.25	41.65	31.10	Clay Loam	D
	5–15	28.41	40.91	30.68	Clay Loam	D
	15–30	32.44	38.21	29.35	Clay Loam	D
	30–60	36.56	35.26	28.18	Clay Loam	D
	60–100	36.57	35.26	28.17	Clay Loam	D
	100–200	35.56	36.32	28.12	Clay Loam	D
Bh13-2-3c	0-5	29.11	41.92	28.97	Clay Loam	D
	5–15	30.30	41.11	28.59	Clay Loam	D
	15–30	33.55	38.99	27.46	Clay Loam	D
	30–60	37.37	36.49	26.14	Clay Loam	D
	60–100	37.55	36.27	26.18	Clay Loam	D
	100–200	36.82	36.89	26.29	Clay Loam	D
Re16-b-235	0-5	25.56	44.32	30.12	Loam	B
	5–15	27.19	43.49	29.32	Clay Loam	D
	15–30	29.67	41.72	28.61	Clay Loam	D
	30–60	30.37	41.30	28.33	Clay Loam	D
	60–100	30.78	40.52	28.70	Clay Loam	D
	100–200	29.55	41.77	28.68	Clay Loam	D

Soil bulk density, which is required as an input value for the simulations in SWAT, is estimated by applying the same procedure employed for soil texture to the bulk density data included in SoilGrids250m [25]. The SPAW tool provided by USDA—Agricultural Research Service in collaboration with the Department of Biological Systems Engineering of the Washington State University (https://hrsl.ba.ars.usda.gov/soilwater/Index.htm, accessed on 15 May 2021) is used to determine soil water content on the basis of clay, sand, and silt fractions.

The saturated hydraulic conductivity K_{sat} is then quantified according to the Campbell model [28]

$$K_{sat_i} = Ce^{-0.025-3.63s-6.9c} \tag{1}$$

where K_{sat_i} (mm/h) is the saturated hydraulic conductivity of the soil layer i, C is a constant assumed equal to 144, and s and c are the average dimensionless fractions of silt and clay in layer i, respectively.

3.2. Climatic Data

Climatic data are retrieved from the Climate Forecast System Reanalysis (CFSR) dataset, provided by the National Centers for Environmental Prediction (NCEP) [29]. NCEP data include daily precipitation, wind, relative humidity, and solar radiation data. The CFSR is designed as a global, high-resolution, coupled atmosphere–ocean–land surface–sea ice system to provide the best estimate of the state of these coupled domains at a spatial resolution of ∼38 km, based on historical data from 1979 to 2014 [30]. Climate data are available for 20 locations close to the target watershed, as displayed in Figure 5.
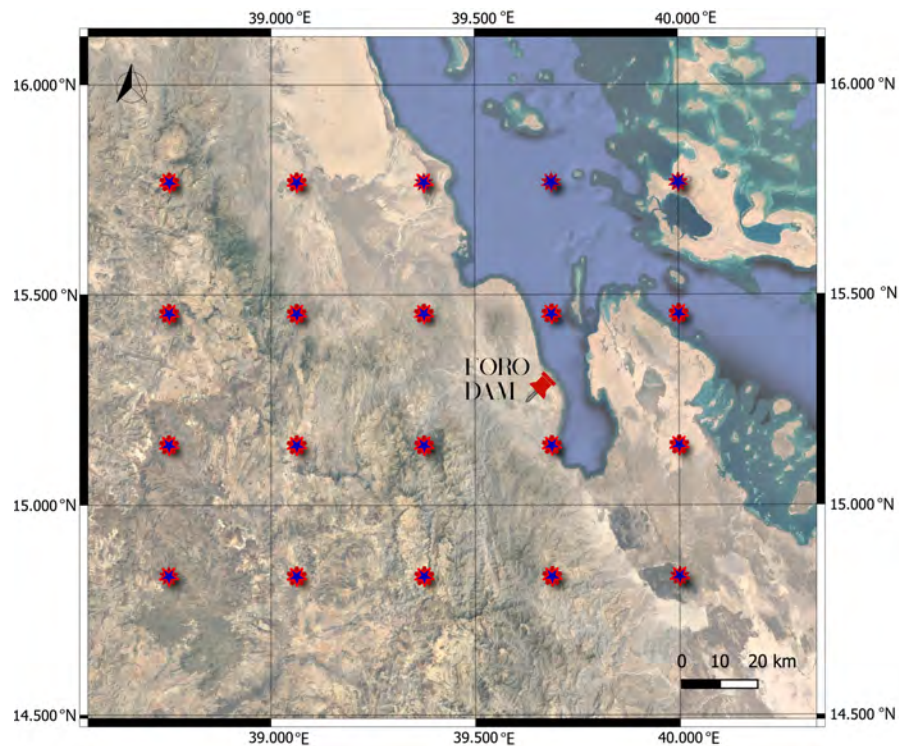

Figure 5. Locations associated with climate data (blue–red markers) provided by NCEP [29] within the area of interest.

4. Preprocessing Analysis

Preprocessing of input data is performed in the QGIS environment using the QSWAT plugin. The Terrain Analysis Using Digital Elevation Models (TauDEM) tool [31] is applied to the DEM in Figure 2 to delineate the watershed and river network. For modeling purposes, the watershed is partitioned into a collection of subbasins. This approach is particularly beneficial when land use and soil properties vary significantly along the catchment area. The basin in Figure 6 is characterized by an extent of 83,075.94 ha and comprises 17 subbasins. As indicated in Figure 6b, the majority of the area encompassed by the watershed is characterized by slopes greater than 25%, located primarily in upland areas, and a land cover represented by low sparse sHRUbs with herbaceous vegetation. Soil types Re16-b-235 and Bd31-2c-11 are dominant in the watershed.
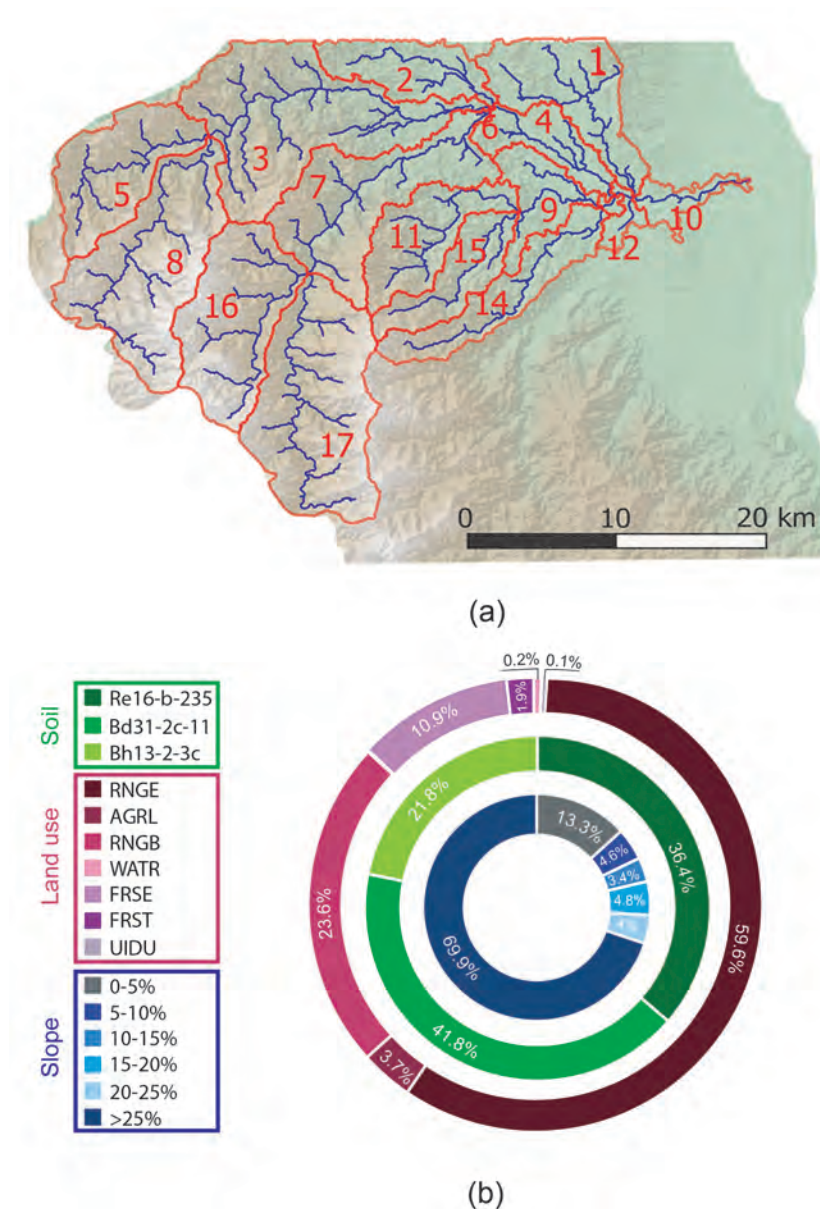
Figure 6. Delineation of the watershed and the river network (**a**), and percentage of the land use, soil, and slope categories across the basin (**b**).

Hydrologic response units (HRUs) are lumped land areas within the subbasin characterized by a unique combination of land cover, soil properties, and slope. The HRUs are defined relying upon the soil map in Figure 4, the land use map in Figure 3, and the slope class percentage of the land area. This enables one to generate portions of the domain characterized (ideally) by uniform properties. Three thresholds are introduced into the model to avoid an excessive number of HRUs and thus reduce the computational load: (*a*) the percentage of land use over the subbasin area; (*b*) the percentage of soil class over land use area; and (*c*) the percentage of slope class over soil area. A threshold value is set to 10% for point (*a*) and to 5% for points (*b*) and (*c*). As such, while HRUs are mainly homogeneous in terms of the three selected properties, they may contain small areas having different properties. The number of HRUs employed in the numerical simulations amounts to 1642.

For the benefit of the interpretation of the results, the subbasins are preliminarily clustered on the basis of topographic, soil properties, and land use information, as well as precipitation data. Clustering aims at assessing whether the similarities between the

subbasins observed in the input data are preserved in the outputs. Rainfall data for the subbasins are obtained by area-weighted averaging of the amount of precipitations provided by SWAT for each subbasin HRU on the basis of climate data from the weather stations used as input dataset. The annual maximum daily precipitation over a 36-year period is interpreted through the generalized extreme value (GEV) distribution [32]

$$F(x) = e^{-(1-\frac{\theta_3}{\theta_2}(x-\theta_1))^{\frac{1}{\theta_3}}} \tag{2}$$

The three parameters $(\theta_1, \theta_2, \theta_3)$ of the cumulative distribution function (CDF) of the GEV distribution in Equation (2) are estimated by the L-moments method. The precipitation corresponding to a return period T_R of 2, 5, 10, 20, and 50 years is evaluated for each subbasin and depicted in Figure 7. Subbasins 8, 11, 15, 16, and 17 exhibit the largest precipitation values for a given return time. The lowest precipitation values are associated with subbasins 2 and 6.
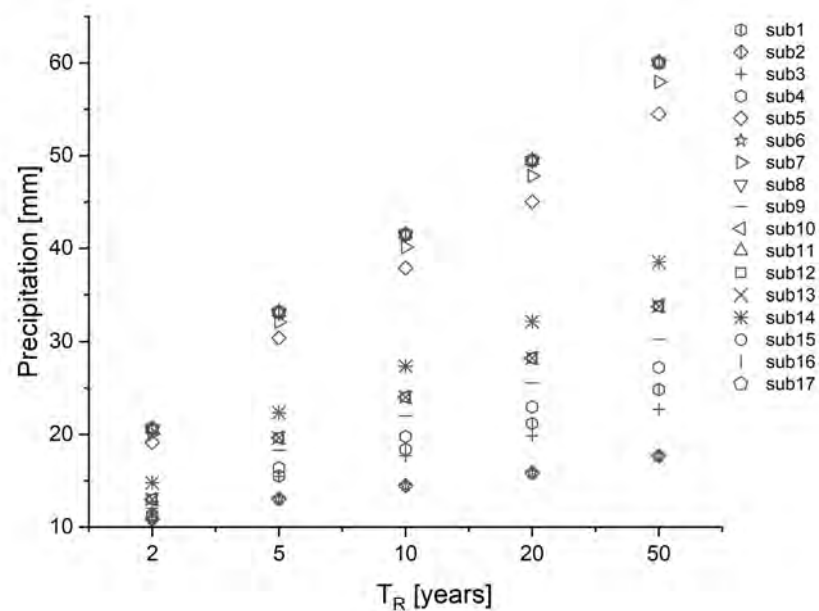

Figure 7. Maximum daily precipitations for a return period T_R of 2, 5, 10, 20, and 50 years for each subbasin. Results are obtained upon interpreting rainfall data through the GEV distribution (Equation (2)).

A hierarchical cluster analysis is performed to find (approximately) homogeneous groups of instances based on the percentage of soil type, land use, and slope characterizing each subbasin displayed in Figure 8b and the corresponding precipitation values in Figure 7. Similarities between objects are used in the delineation of clusters relying upon the hierarchical cluster analysis in OriginLab [33]. The spatial distribution of the subbasins with similar features is displayed in Figure 8a.
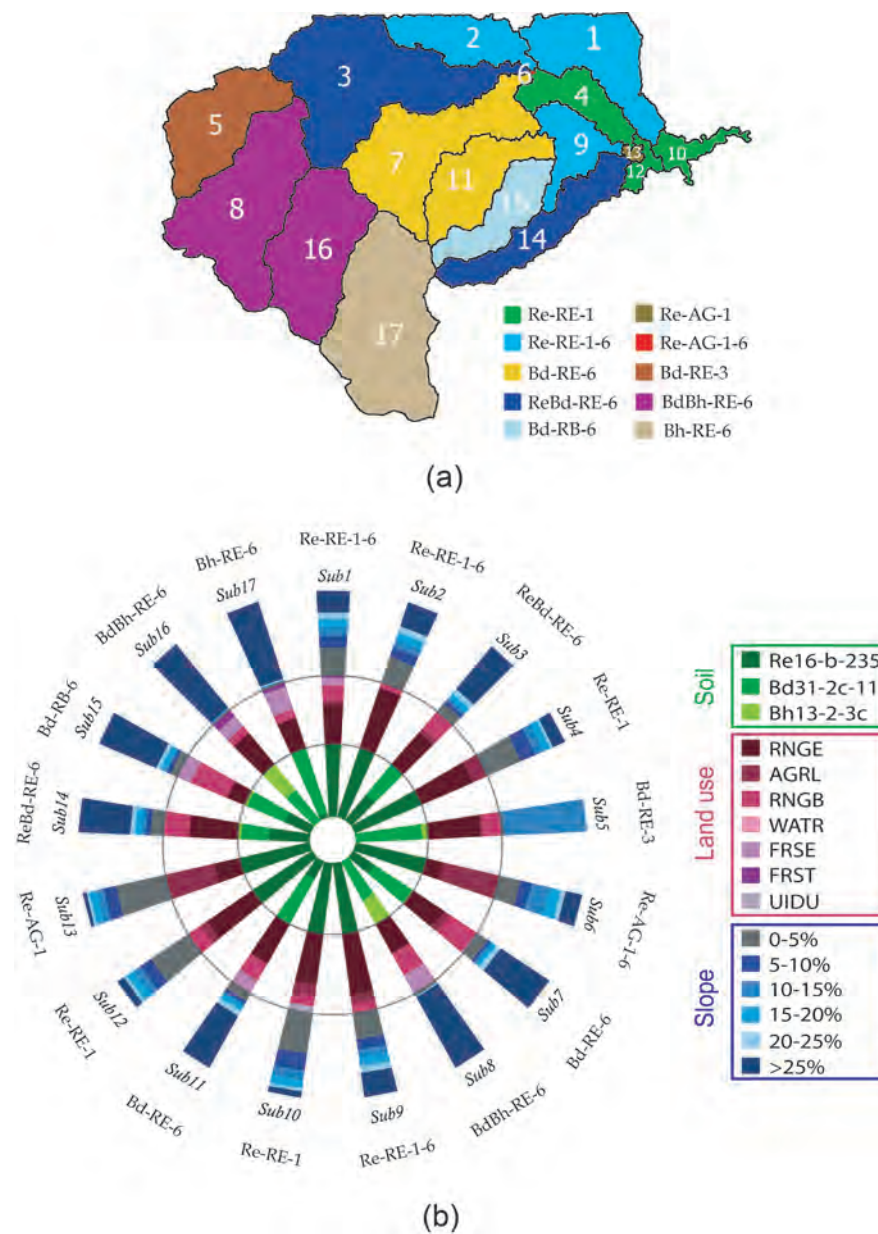
Figure 8. Clustering of the subbasins exhibiting similar features in terms of soil properties, land use, topographic slope, and precipitations (**a**). Panel (**b**) indicates the percentage of each soil group, land use category, and slope.

Each group of subbasins is labeled with a code where the first and the second term indicate the soil type (Re=Re16-b-235, Bd=Bd31-2c-11, Bh=Bh13-2-3c) and the land use category (RE = RNGE, AG = AGRL, RB = RNGB, W = WATR, FE = FRSE, FT = FRST, U= UIDU), respectively, and a number from 1 to 6 is attributed to slope range (in ascending order). When two soil categories are characterized by a similar percentage, the two corresponding acronyms are jointly used to codify the cluster.

5. Hydrological Model

Numerical results are obtained using the SWAT hydrological model [17]. The hydrology of the watershed is simulated by two major phases of the hydrological cycle: (1) the land phase, which regulates the amount of water and sediment loading to the main channel in each subbasin, and (2) the routing phase, estimating the movement of water and sediments through the channel network to the outlet [17]. The water mass balance equation [17] reads as

$$SW_t = SW_0 + \sum_{i=1}^{t}(P_{day} - Q_{surf} - E_a - w_{seep} - Q_{gw}) \tag{3}$$

where t is time (expressed in days), SW_t and SW_0 (mm) are the soil water content at time t and the initial soil water content on day i, respectively, P_{day} corresponds to the amount (mm) of precipitation on day i, Q_{surf} (mm) is the runoff on day i, E_a (mm) represents the evapotranspiration on day i, w_{seep} (mm) is the quantity of water reaching the vadose zone on day i, and Q_{gw} (mm) is the base flow on day i. The model formulation is described in the following paragraphs.

5.1. Surface Processes: Runoff and Evapotranspiration

Surface runoff is evaluated through a modification of the Soil Conservation Service (SCS) curve number method proposed by the USDA [34] for each HRU and is routed to obtain Q_{surf} for the entire watershed. Surface runoff is estimated as

$$Q_{surf} = \frac{(P_{day} - I_a)^2}{P_{day} - I_a + S} \tag{4}$$

where I_a is the initial abstraction prior to runoff (mm) and S corresponds to the retention parameter quantified as a function of the curve number CN [34].

$$S = 25.4\left(\frac{1000}{CN} - 10\right) \tag{5}$$

where $0 \leq CN \leq 100$ is a dimensionless model parameter. Runoff occurs only when $P_{day} > I_a$, the initial abstraction I_a, being generally approximated as 20% of the retention parameter. Evapotranspiration (denoting the collection of all processes by which the water is removed from the surface, including evaporation from plants and soil, transpiration, and sublimation) is estimated through the Penmann–Monteith method [35]. This approach accounts for the energy needed for evaporation and water vapor removal, as well as aerodynamic and surface resistance, and is formulated as

$$\lambda E = \frac{\Delta(H_{net} - G) + \rho_{air}c_p(\frac{e_z^0 - e_z}{r_a})}{\Delta + \gamma(1 + \frac{r_c}{r_a})} \tag{6}$$

where λE is the latent heat flux density (MJm^{-2}d^{-1}), E corresponds to the depth rate evaporation (mmd^{-1}), Δ is the slope of the saturation vapor pressure–temperature curve (kPa°C^{-1}), H_{net} represents the net radiation (MJm^{-2}d^{-1}), G is the heat flux density to the (MJ m^{-2}d^{-1}), ρ_{air} is the air density (kg m^{-3}), c_p is the specific heat at constant pressure (MJ kg^{-1}°C^{-1}), e_z^0 and e_z are the saturation and the water vapor pressure of air at height z (kPa), respectively, γ is the psychrometric constant (kPa°C^{-1}), and r_c and r_a correspond to the plant canopy resistance and the aerodynamic resistance (diffusion resistance of the air layer) (sm^{-1}), respectively.

The soil evaporative demand is evaluated for each layer of the soil profile E_{sk} as function of the evaporative demand of the upper and lower boundary of the soil layer k, E_{sku}, and E_{skl}, respectively, and a model parameter (*esco*) (see Appendix A for details) [17].

$$E_{sk} = E_{skl} - E_{sku} \cdot esco \tag{7}$$

5.2. Subsurface Water Balance

Infiltration is estimated as the difference between the amount of rainfall and surface runoff. The soil profile is partitioned into multiple layers. Here, we rely on six layers (Table 3). Evaporation, plant uptake, transpiration, lateral flow (i.e., the subsurface flow occurring at a depth between the surface and the zone where the host porous medium is fully saturated with water), and the percolation to deeper layers are considered as soil

water processes. The potential water uptake from the soil surface is quantified for each soil layer *k* as the difference between the potential water uptake for the upper and lower boundary of layer *k*, both expressed as a function of the maximum plant transpiration on a given day. If the upper layers of the soil profile do not contain enough water to satisfy the potential water uptake of layer *k*, the potential water uptake can be adjusted by introducing the plant uptake compensation factor *epco* (see Appendix A), according to [17].

$$w'_{up,k} = w_{up,l} - w_{up,u} + w_d \cdot epco \tag{8}$$

where $w'_{up,k}$ is the adjusted potential water uptake of layer *k*, $w_{up,u}$ and $w_{up,l}$ are the potential water uptake for the upper and lower boundary, respectively, and w_d represents the water uptake demand not met by overlying soil layers. The compensation factor *epco* ranges between 0.01 and 1. Percolation is quantified for each soil layer and takes place only when the water content of layer *k* exceeds its field capacity and the layer above is not saturated.

Two types of aquifers are simulated in SWAT for each subbasin: (*i*) the shallow aquifer, that is unconfined and contributes to the flow in the main channel of the subbasin, and (*ii*) the deep confined aquifer contributing also to the streamflow outside the watershed. Water fluxes in the shallow aquifer are subject to various processes such as evaporation, base flow to the channel, and seepage to the deep aquifer. The water percolating from the lowest layer of the soil profile flows through the vadose zone and recharges the shallow aquifer. The aquifer recharge is simulated by relying on the exponential decay weighting function proposed by Venetis [36], describing a setting where the recharge is not instantaneous and exhibits days of delay. For each subbasin, the recharge is estimated as [17].

$$w_{rchrg,i} = (1 - e^{-\frac{1}{\delta_{gw}}})w_{seep} + e^{-\frac{1}{\delta_{gw}}} w_{rchrg,i-1} \tag{9}$$

where $w_{rchrg,i}$ and $w_{rchrg,i-1}$ (mm) are the recharge of the aquifer on day *i* and day (*i* − 1), respectively, δ_{gw} (days) is the delay time of the overlying soil profile, and w_{seep} (mm) is the total amount of water exiting from the bottom of the soil profile on day *i*. The total daily recharge $w_{rchrg,i}$ is divided between the shallow and deep aquifer. The contribution to the latter is estimated as $\beta_{deep} \cdot w_{rchrg,i}$ with $\beta_{deep} \in [0,1]$.

5.3. Erosion

Erosion and sediment yield are simulated for each HRU with the modified universal soil loss equation (MUSLE) [37] that provides an appraisal of the average annual gross erosion as a function of the surface runoff. For a selected HRU, the daily sediment yield y_{sed} (metric tons) is estimated as [17]

$$y_{sed} = 11.8(Q_{surf} \cdot q_{peak} \cdot A_{HRU})^{0.56} K_{usle} \cdot C_{usle} \cdot P_{usle} \cdot LS_{usle} \cdot CFRG \tag{10}$$

where q_{peak} is the peak runoff rate (m^{3}s^{-1}), A_{HRU} represents the area of the HRU (ha); K_{usle} corresponds to the universal soil loss equation (USLE) soil erodibility factor (metric ton m^2 hr/m^3 −metric ton cm), C_{usle} is the USLE cover and management factor, P_{usle} is the USLE support practice factor, LS_{usle} is the USLE topographic factor, and *CFRG* is the coarse fragment factor. Note that the parameter K_{usle} describes the erodibility of the soil depending on the properties of the soil itself. It can be estimated as a function of the soil texture [38].

The USLE cover and management factor is defined as the ratio between the soil loss in cropped and clean-tilled land, indicating the effect of the plant canopy on the soil erosion. The support practice factor P_{usle} represents the ratio of soil loss with a specific support practice, including the contour tillage and terrace systems, to the corresponding loss with up-and-down slope culture [17]. The specific value of P_{usle} depends on the support practice and increases with the land slope.

Sediment transport in the stream network is the result of landscape erosion and channel degradation. The latter depends on the stream power, which exerts an erosive force on the sides and the bottom of the channel, and the composition of the channel bank and bed sediments. Sediment yield from the landscape is evaluated by the MULSE model [37] and is lagged and routed through the grass waterway before reaching the channel. The sediment transport in the channel comprises degradation and deposition, acting simultaneously in the reach. Occurrence of either of these processes is determined by comparing the concentration of the sediments in the reach at the beginning of the time step $C_{s,i}$ with the maximum sediment concentration $C_{s,max}$. Deposition is the main phenomenon if $C_{s,i} > C_{s,max}$, while degradation dominates when $C_{s,i} < C_{s,max}$. The maximum sediment concentration is estimated by the stream power equation proposed by Bagnold [39] where $C_{s,max}$ depends on the peak channel velocity v_{pk} according to

$$C_{s,max} = c_{sp} \cdot v_{pk}^{spexp} \tag{11}$$

where c_{sp} and $spexp$ are model parameters (see Appendix A).

6. Results

The results presented here are obtained through numerical simulations performed in the SWAT computational suite relying on the hydrological model described in Section 5. They comprise a temporal window from 1988 to 2000 with a warm-up period of two years. We investigate the spatial variation in surface-level hydrological components, surface runoff, and the river network, which includes channel discharge and sediment yield. Target hydrologic variables are first evaluated for all subbasins using the default model parameters (see Tables 4 and 5). All results are provided as a time series of daily data. The highest fifth-percentile of output values are considered for each subbasin, to enable analysis of events leading to the most significant flow and land erosion scenarios.
The distribution of daily runoff values associated with the highest fifth percentile is evaluated and depicted in Figure 9b. Here, the subbasins exhibiting a similar distribution of Q_{surf} are grouped according to the hierarchical cluster analysis performed upon relying on OriginLab [33]. The curve number (*CN*) for each subbasin in Figure 9a is estimated as the area-weighted average of the curve number value assigned to each HRU associated with the subbasin.
Subbasin 2 is characterized by infrequent events of low-magnitude surface runoff ($Q_{surf} < 1$ mm) observed only after more intense rainfall days, mainly observed in 1995. This behavior is related to a combination of low-intensity precipitation (see Figure 7), a mostly flat surface, and low curve number values (see Figure 9a). A similar result is found for Subbasin 3, which exhibits Q_{surf} values larger than those associated with Subbasin 2. These display a range of variation between 10^{-6} and 10^2 mm, consistent with a higher *CN* characterizing this region of the watershed. Significant surface runoff is slightly more frequent in the clusters of Subbasins sub1–sub14, sub6–sub11, sub15–sub16 (with daily maximum values of 10^2 mm), and sub3 (up to 10 mm). A higher number of days with more significant runoff is observed in sub5–sub12, sub7–sub8–sub17, and sub10, the latter representing the subbasin with the most significant runoff events during the simulation period. This observation is consistent with the higher *CN* value assigned to this subcatchment (Figure 9a). Considering that the curve number depends on land use, soil properties, and slope, the high *CN* in sub10 is possibly due to the *UIDU* land use category and Re16-b-235 soil type characterizing this zone. As seen in Table 2, the code *UIDU* indicates land cover with rocky sand, which is characterized by low infiltration capacity. For all subbasins, the greatest amount of runoff is associated with infrequent high intensity rain events.
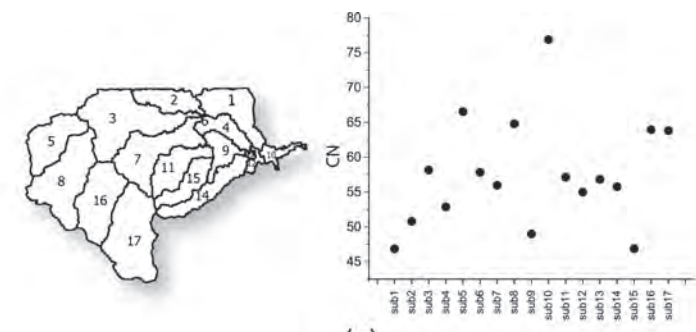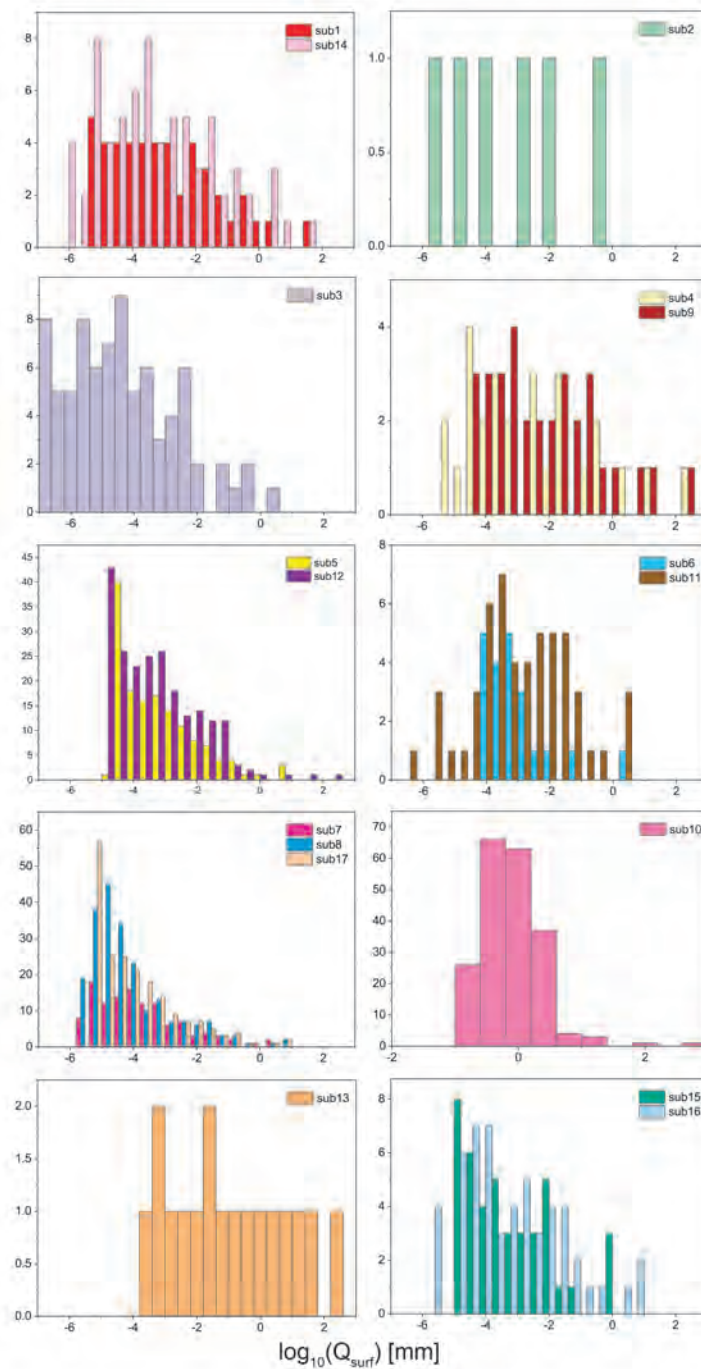
Figure 9. Average curve number associated with each subbasin (**a**) and histogram of the highest fifth percentile of the daily Q_{surf} for each subbasin (**b**).

Sediment transported with water (y_{sed}) out of the reference channel for each subbasin is assessed, and results corresponding to the highest fifth percentile are depicted in Figure 10. The results are grouped according to subbasins characterized by a similar distribution of daily y_{sed} across the considered period. Clustering of the outputs is performed upon relying on the hierarchical cluster analysis embedded in OriginLab [33].

The lowest amount of transported sediments takes place in subbasins 1 and 2. Note that subbasin 1 and 14 feature similar values in terms of runoff (see Figure 9). However, the higher slope range characterizing sub14 leads to a significant difference in terms of transported sediments. Daily sediment rates in the uplands (sub8 and sub17) vary between 10^3 and 10^5 tons. Subbasins 8 and 17 are subject to the highest degradation as a result of a higher discharge rates. The remaining subbasins are characterized by medium–high sediment transport, ranging from 10 to 10^5 tons. Most of the subbasins located in the central part of the watershed (sub3-sub4-sub9-sub11-sub12-sub14) show similar behaviors in terms of sediment transport. These areas of the basin are characterized by similar degrees of channel degradation and by the same predominant land use category (RNGE).
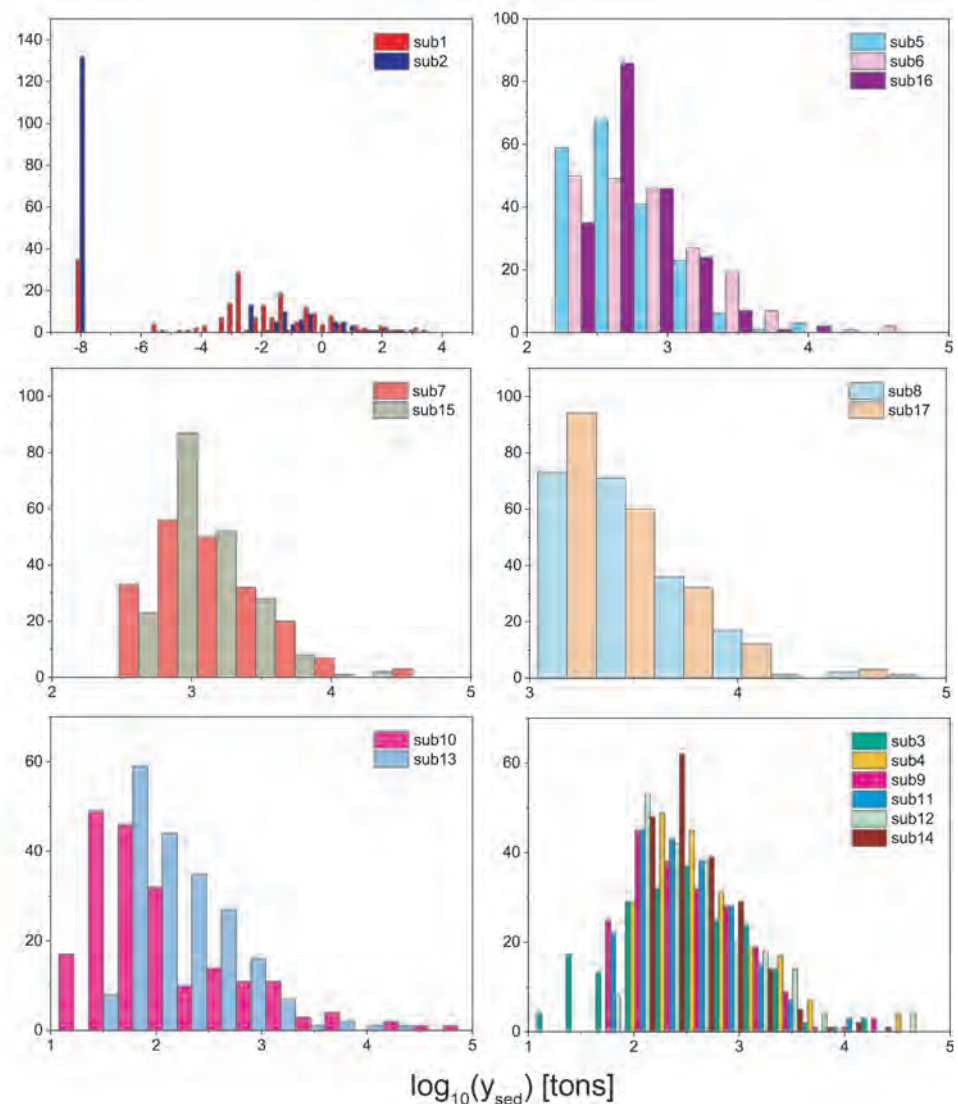

Figure 10. Histogram of the highest fifth percentile of the daily values of y_{sed} of the reference channel of each subbasin.

River discharge along the entire watershed exhibits a behavior similar to sediment transport. The highest value of q_r is found at the outlet of the hydrological basin, within subbasin 10. The cumulative distribution function (CDF) of the highest fifth-percentile daily discharge rate during the simulation period is displayed in Figure 11. We can notice that q_r ranges from 1.5 to 250 m^3/s, most values being lower than ≈ 50 m^3/s.
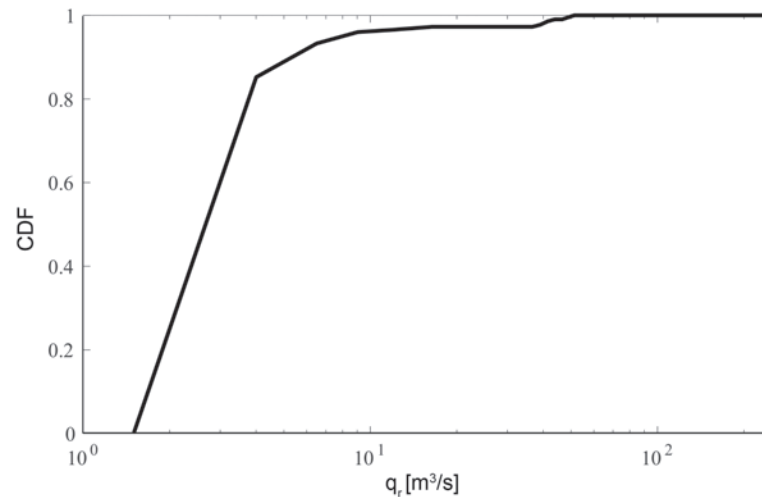

Figure 11. Cumulative distribution function (CDF) of the highest fifth percentile of the daily values of q_r at the outlet (sub10).

Sensitivity Analysis

A sensitivity analysis is performed to assess the impact of the model parameters on the outputs of interest. The model parameters accounted for in the sensitivity analysis and their features are listed in Tables 4 and 5. Representative parameters for the major hydrologic processes, such as runoff, evapotranspiration, infiltration, channel flow, sediment transport, and aquifer flow, are included in the analysis. For the purpose of the analysis, the majority of the parameters are subject to percentage (pctchg) variations in a range between -25% and 25%. A few parameters are varied in absolute value (absval) across the corresponding support. The variation of a given parameter is applied uniformly to any given HRU.

Simulations are performed across a 7-year period (1988–1994, with 2 years of warm-up) to reduce the computational load.

Table 4. Hydrological parameters, corresponding support (i.e., range of variability), and type of variation used in the sensitivity analysis.

Type Parameter	Name	Definition	Default Value	Range	Type Variation
Surface runoff	CN2	SCS runoff curve number for moisture condition II	59 [a]	[−25%, 25%]	pctchg [b]
	surlag	Surface runoff lag coefficient	4	[−25%, 25%]	pctchg
Channel	ovn	Manning's roughness coefficient	0.365	[−25%, 25%]	pctchg
	trnsrch	Fraction of transmission losses from main channel that enter deep aquifer	0	[−25%, 25%]	pctchg
Evapo-transpiration	esco	Soil evaporation compensation factor	0.95	[0, 1]	absval [c]
	epco	Plant evaporation compensation factor	1	[0, 1]	absval
	evrch	Reach evaporation adjustment factor	1	[0, 1]	absval
Percolation	perco	Percolation coefficient-adjusts soil moisture for percolation to occur	1	[−25%, 25%]	pctchg

[a] Default value for the entire watershed. [b] Percentage variation. [c] Absolute value variation.

Table 5. Hydrological parameters, corresponding support (i.e., range of variability), and type of variation used in the sensitivity analysis.

Type Parameter	Name	Definition	Default Value	Range	Type Variation
Sediments	spcon	Linear parameter for calculating the maximum amount of sediment that can be re-entrained	0.0001	[−25%, 25%]	pctchg
	D50	Median particle diameter of sediment (μm)	12	[−25%, 25%]	pctchg
	spexp	Exponent parameter for calculating sediment reentrained in channel sediment routing	1	[−25%, 25%]	pctchg
	p_usle	USLE equation support practice factor	0.875	[−25%, 25%]	pctchg
	prf	Peak rate adjustment factor for sediment routing in the main channel	1	[−25%, 25%]	pctchg
	adj_pkr	Peak rate adjustment factor for sediment routing in the subbasin (tributary channels)	1	[0.5, 1]	absval
Groundwater	revap_co	Groundwater revap coefficient	0.02	[−25%, 25%]	pctchg
	revap_min	Threshold depth of water in the shallow aquifer for revap to occur (mm)	5	[−25%, 25%]	pctchg
	alpha_bf	Base flow alpha factor (days)	0.05	[-25%, 25%]	pctchg

A short description of the physical meaning of the parameters is provided in Tables 4 and 5. Additional details are given in Appendix A.

The AMAE global sensitivity index is used to estimate the influence of each model parameter on the assessed hydrological quantities. This metric has been introduced by Dell'Oca et al. [40] and allows quantifying the effect of the uncertainty associated with a given model parameter x_i on the expected value of a model output variable of interest, y. It is defined as

$$
AMAE_{x_i} = \begin{cases} \frac{1}{|y_0|} E[|y_0 - E[y|x_i]|], & \text{if } y_0 \neq 0 \\ E[|y_0 - E[y|x_i]|], & \text{if } y_0 = 0 \end{cases} \tag{12}
$$

where $E[\cdot]$ denotes expected value, $E[y|x_i]$ represents the conditioning on x_i, and y_0 is the unconditional average of y, as a result of the uncertainty associated with the complete set of model parameters. The AMAE sensitivity metric is evaluated, considering as output the maximum value of the quantity of interest over the simulation period for each combination of the model parameters sampled from a uniformly distributed supporting set. A total of 600 realizations was used to estimate the AMAE index. Quantities of interest considered in the analysis are river discharge q_r, transported sediments y_{sed}, and surface runoff Q_{surf}. With reference to surface runoff, the curve number is univocally identified as the most relevant parameter for all the subbasins, while the remaining parameters are characterized by low values of the AMAE index (Figure 12). According to Equations (4) and (5), CN and Q_{surf} are linked by a direct proportionality (see also Figure 13). In the subbasins 1 and 2, surface runoff occurs only for $CN > 55$ and $CN > 60$, respectively, as shown in Figure 13a. An overlap of the curve representing runoff as a function of the average curve number is noted in Figure 13b,c for sub5–sub8–sub16–sub17 and sub7–sub11–sub14, these regions being characterized by a similar average curve number in the default parameterization (see Figure 9a).
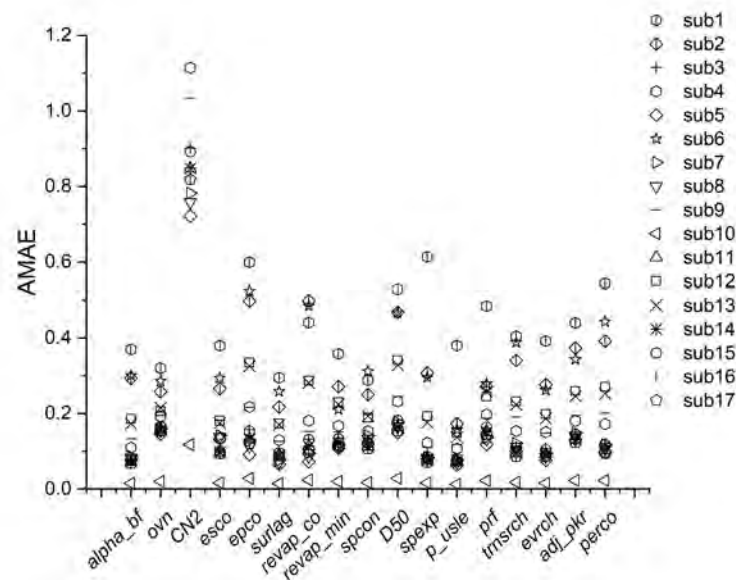

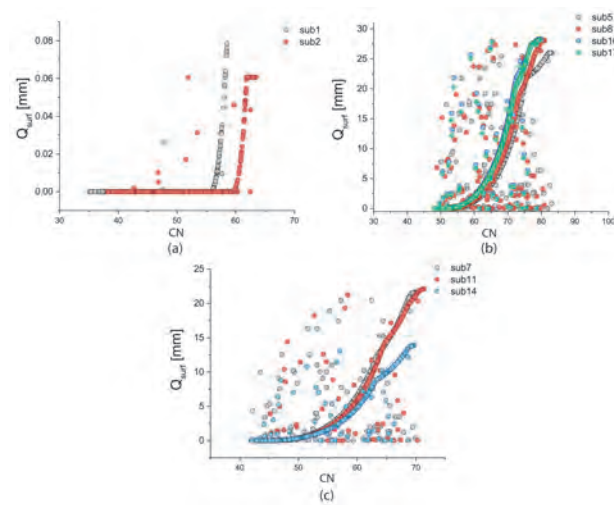**Figure 12.** AMAE index for Q_{surf} of the model parameters.

Figure 13. Scatterplot of the average curve number and the maximum runoff for each combination of model parameters for different subbasins: subbasin 1 and 2 (**a**); subbasins 5, 8, 16, and 17 (**b**); subbasins 7, 11, and 14 (**c**).

The marked importance of *CN* in governing runoff values propagates to outflow rates and sediment discharges. Results in Figure 14a,b suggest that the curve number is the most influential parameter driving the expected value of the maximum outflow rate during the simulation period for all subbasins, except for sub1. In subbasin 1, the reach evaporation adjustment factor has a greater influence on river discharge, while the influence of all the remaining hydrological parameters is essentially negligible. Note that values of the maximum discharge in this subbasin are typically lower than 0.1 m^3/s.

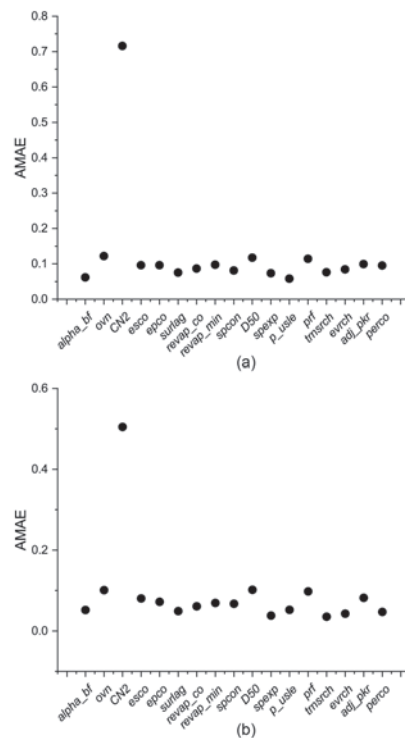**Figure 14.** AMAE index for maximum daily q_r (**a**) and y_{sed} (**b**) at the outlet (sub10).

7. Conclusions

The study tackles the investigation of hydrological processes taking place in a basin in the Foro region of Eritrea (East Africa). The work is motivated by the need to quantify river discharge and sediment transport at the Foro Dam. To this end, we build a hydrological model based on the widely used and tested SWAT computational suite [17]. The model is parameterized using remote sensing data and other available datasets. The spatial variation of the hydrological quantities across the catchment area provides an overview of the main surface processes taking place throughout the entire basin. In the preprocessing phase, sub-basins are clustered based on input data, including information on land use, soil properties, topographic slope, and precipitation. Lack of observed data does not allow calibration of the hydrological model parameters. The distribution of river discharge, transported sediment, and runoff over an 11-year period is evaluated using the default parameter values in SWAT. Under the default parameterization, maximum observed outflow rates are in the order of 100 m^3/s at the outflow section and maximum values of daily sediment transported at the outflow section are approximately 10^5 tons. Significant uncertainty affects these values, also due to the observation that the developed SWAT model assumes a daily temporal scale that cannot capture the effect of short-duration and high-intensity events. Modeling on a smaller timescale will be the subject of future investigations. We observed that the northernmost region (subbasins 1 and 2) is characterized by the lowest water fluxes. This stems from the combined effect of low-intensity rainfall events and an overall flat surface. Sediment transport and surface runoff are processes of minor relevance in these regions of the watershed.

Otherwise, significant runoff leading to degradation due to erosive phenomena is observed in the upland subbasins (sub8–17). Thus, fine-scale modeling and field measurements should specifically target this area. A detailed global sensitivity analysis is performed to evaluate the influence of the uncertain model parameters on the assessed hydrological quantities. The curve number (*CN*) markedly dominates runoff along the watershed. This result suggests that *CN* could be considered as the key parameter to be estimated through model calibration to constrain surface water processes. In the absence of direct observations of river discharges or other hydrological fluxes, the use of satellite images will be considered in future research efforts.

Appendix A. Model Parameters

We introduce here in more detail the model parameters employed in the sensitivity analysis (see Tables 4 and 5).

Appendix A.1. Surface Processes

Surface runoff and stream flow parameters are considered in this section. The runoff curve number for moisture condition II (*CN2*) is a function of the permeability of soils, land use, and prior soil water conditions. It controls the amount of the surface runoff according to Equations (4) and (5).

Surlag regulates the fraction of the surface runoff that enters the reach on any day: for a given time concentration, i.e., the amount of time the water needs to reach the outlet in each subbasin, as *surlag* increases, more water is released into the channel.

The Manning's roughness coefficient (*ovn*) controls the evaluation of overland flow velocity v, according to [17]:

$$v = \frac{q^{0.4} \cdot spl^{0.3}}{ovn^{0.6}} \tag{A1}$$

where spl is the average slope in the subbasin (mm^{-1}) and q represents the average overland flow rate ($\text{m}^3 \text{ s}^{-1}$). Water losses from the stream network due to evaporation and percolation are also considered. The reach evaporation adjustment factor *evrch* allows reducing the reach evaporation that is generally overestimated with the original equation in the arid zones. The parameter *trnsrch* specifies the fraction of permanent transmission losses from the main channel network to deep aquifers. The parameter accounts for water volume fraction that cannot be considered to flow back onto the surface via aquifer-river interactions.

Appendix A.2. Soil and Subsurface Flow

Several parameters are employed to regulate water fluxes from groundwater and soil. The groundwater revap coefficient *revap_co* regulates the water that can be removed for evaporation from the aquifer by deep-rooted plants when the soil profile overlying the aquifer is dry. When *revap_co* tends to 1, the rate of transfer from the shallow aquifer to the root zone approaches the rate of potential evapotranspiration. The threshold depth of water in the shallow aquifer for *revap_min* controls fluxes from the shallow aquifer to the unsaturated zone: the water moves only if the shallow aquifer contains a volume of water equal to or greater than *revap_min*.

The baseflow recession constant (*alpha_bf*) affects the groundwater flow response to changes in recharge. As *alpha_bf* increases, the groundwater flow into the main channel decreases according to Equation (A2).

$$Q_{gw,t} = Q_{gw,0} e^{-alpha\_bf \cdot t} \tag{A2}$$

where $Q_{gw,t}$ and $Q_{gw,0}$ are the flux terms describing groundwater recharge to the main channel at time t and at the beginning of the recession, respectively.

Evapotranspiration from soil layers is considered by several parameters. The soil evaporation compensation factor *esco* is employed to include the effects of capillary action, crusting, and cracks in the quantification of the soil evaporative demand distribution. As *esco* reduces, the evaporative demand is increasingly satisfied by the lower soil layer. The plant evaporation compensation factor *epco* enables the lower soil layer to meet the water uptake demand. The amount of water uptake needed in a given day depends on the water available in the soil and the quantity required by the plants for transpiration. When the water content of the upper soil layer is insufficient to satisfy the potential water uptake, the lower layer can compensate. As *epco* tends to 1, lower layers of soil are increasingly allowed to contribute and compensate water uptake.

Appendix A.3. Erosion

Parameters related to hillslope erosion and sediment transport in the stream network are here listed. The parameters $spcon$ and $spexp$ quantify the maximum amount of sediment that can be transported from a reach segment according to Equation (11).

The median particle diameter of sediments $D50$ within a subbasin can be estimated as an exponential function of the percentage of clay (m_c), sand (m_s), and silt (m_{silt}) of the surface soil layer, as [17]

$$D50 = exp\left(0.41\frac{m_c}{100} + 2.71\frac{m_{silt}}{100} + 5.7\frac{m_s}{100}\right). \tag{A3}$$

As defined in Section 5, p_usle represents the ratio of soil loss with a specific practice, including contour tillage, stripcropping on the contour, and terrace systems, and with up-and-down slope culture used to quantify the sediment yield; see Equation (10). Sediment routing depends on the mean daily flow rate and the peak flow rate, the latter being defined as the product between the peak rate adjustment factor prf and the average flow rate. The peak rate adjustment factor for sediment routing in the subbasin adj_pkr affects the amount of erosion generated in the HRUs.

References

1. Mutunga, C.; Zulu, E.M.; De Souza, R.M. Population dynamics, climate change and sustainable development in Africa. 2012. Available online: https://www.africaportal.org/publications/population-dynamics-climate-change-and-sustainable-development-in-africa/ (accessed on 15 May 2021).
2. Zeraebruk, K.N.; Mayabi, A.O.; Gathenya, J.M. Assessment of Water Resources and Analysis of Safe Yield and Reliability of Surface Water Reservoirs of Asmara Water Supply System. *Environ. Nat. Resour. Res.* **2017**, *7*, 45.
3. Tewolde, M.G.; Cabral, P. Urban sprawl analysis and modeling in Asmara, Eritrea. *Remote Sens.* **2011**, *3*, 2148–2165.
4. Polimi. VITAE. Available online: https://www.mecc.polimi.it/us/about-us/news/progetto-vitae-new-strategies-for-a-sustainable-valorisation-of-the-eritrean-heritage/ (accessed on 15 February 2022).
5. Bortolotto, S.; Cattaneo, N.; Massa, S. Seasonal watercourses as a source of wealth and a cause of destruction: The water management in Adulis (Eritrea) in antiquity and today. *Larhyss J.* **2021**, *47*, 25–38.
6. Bortolotto, S.; Cheli, F. Eritrean Mobility and Cultural Heritage. New Frontiers of the Horn of Africa. An overview of the project. *E Motion Eritrean Mobil. Cult. Heritage. New Front. Horn Afr.* **2021**, *17*, 23.
7. Arnold, J.G.; Fohrer, N. SWAT2000: Current capabilities and research opportunities in applied watershed modelling. *Hydrol. Process. Int. J.* **2005**, *19*, 563–572.
8. Rockwood, D.M.; Davis, E.M.; Anderson, J.A. *User Manual for COSSARR Model*; US Army Engineer Division, North Pacific: Oregon, Portland, 1972.
9. Sugawara, M. Tank model and its application to Bird Creek, Wollombi Brook, Bikin River, Kitsu River, Sanaga River and Nam Mune. *Res. Notes Natl. Res. Cent. Disaster Prev.* **1974**, *11*, 1–64.
10. Hydrologic Engineering Center (US); Water Resources Support Center (US). *HEC-1 Flood Hydrograph Package: Users Manual*; US Army Corps of Engineers, Water Resources Support Center, Hydrologic: Fort Belvoir, VA, USA, 1981.
11. Williams, J.; Hann, R. HYMO: Problem-oriented language for hydrologic modeling-User's manual. USDA. *ARS-S-9* **1973**, *45*, 1–76.
12. Abbott, M.; Bathurst, J.; Cunge, J.; O'connell, P.; Rasmussen, J. An introduction to the European Hydrological System—Systeme Hydrologique Europeen,"SHE", 2: Structure of a physically-based, distributed modelling system. *J. Hydrol.* **1986**, *87*, 61–77.
13. Beven, K.; Calver, A.; Morris, E. *The Institute of Hydrology Distributed Model*; Institute of Hydrology: Wallingford, UK, 1987.
14. Knisel, W.G. *CREAMS: A Field Scale Model for Chemicals, Runoff, and Erosion from Agricultural Management Systems*; Number 26, Department of Agriculture, Science and Education Administration: Hyattsville, MD, USA, 1980; pp. 1–113.
15. Leonard, R.; Knisel, W.; Still, D. GLEAMS: Groundwater loading effects of agricultural management systems. *Trans. ASAE* **1987**, *30*, 1403–1418.
16. Williams, J.R.; Jones, C.; Dyke, P.T. A modeling approach to determining the relationship between erosion and soil productivity. *Trans. ASAE* **1984**, *27*, 129–0144.
17. Neitsch, S.L.; Arnold, J.G.; Kiniry, J.R.; Williams, J.R. *Soil and Water Assessment Tool Theoretical Documentation Version 2009*; Technical Report, Texas Water Resources Institute: College Station, TX, USA, 2011; pp. 1–618.
18. Hussainzada, W.; Lee, H.S. Hydrological Modelling for Water Resource Management in a Semi-Arid Mountainous Region Using the Soil and Water Assessment Tool: A Case Study in Northern Afghanistan. *Hydrology* **2021**, *8*, 16.
19. Emiru, N.C.; Recha, J.W.; Thompson, J.R.; Belay, A.; Aynekulu, E.; Manyevere, A.; Demissie, T.D.; Osano, P.M.; Hussein, J.; Molla, M.B.; et al. Impact of Climate Change on the Hydrology of the Upper Awash River Basin, Ethiopia. *Hydrology* **2022**, *9*, 3.

20. Saade, J.; Atieh, M.; Ghanimeh, S.; Golmohammadi, G. Modeling Impact of Climate Change on Surface Water Availability Using SWAT Model in a Semi-Arid Basin: Case of El Kalb River, Lebanon. *Hydrology* **2021**, *8*, 134.

21. Ibrahim, B.; Wisser, D.; Barry, B.; Fowe, T.; Aduna, A. Hydrological predictions for small ungauged watersheds in the Sudanian zone of the Volta basin in West Africa. *J. Hydrol. Reg. Stud.* **2015**, *4*, 386–397.

22. Carannante, A.; Flaux, C.; Morhange, C.; Zazzaro, C. Adulis in its regional maritime context. apreliminary report of the 2015 field season. *Newsl. Di Archeol. CISA* **2015**, *6*, 279–294.

23. Ogbazghi, W. Agro-climatic and environmental hazards and mitigation measures for the Northern and Southern Red Sea zone administrations of Eritrea. *J. Eritrean Stud.* **2018**, *8*, 85–131.

24. Dile Yihun, T.S.R. QGIS Interface for SWAT+: QSWAT+; 2021; pp. 1–136. Available online: https://docplayer.net/204909159-Qgis-interface-for-swat-qswat.html (accessed on 15 May 2021).

25. Tarboton, D. SOILGRIDS. Available online: https://soilgrids.org/ (accessed on 15 May 2021).

26. Batjes, N.H.; Ribeiro, E.; Van Oostrum, A. Standardised soil profile data to support global mapping and modelling (WoSIS snapshot 2019). *Earth Syst. Sci. Data* **2020**, *12*, 299–320.

27. Wang, P.L.; Feddema, J.J. Linking global land use/land cover to hydrologic soil groups from 850 to 2015. *Glob. Biogeochem. Cycles* **2020**, *34*, e2019GB006356.

28. Campbell, G.S. *Soil Physics with Basic, Transport Models for Soils-Plant Systems*; Technical Report, Elsevier: Amsterdam, The Netherlands, 1985; Volume 14, pp. 1–150.

29. Saha, S.; Moorthi, S.; Wu, X.; Wang, J.; Nadiga, S.; Tripp, P.; Behringer, D.; Hou, Y.T.; Chuang, H.Y.; Iredell, M.; et al. The NCEP climate forecast system version 2. *J. Clim.* **2014**, *27*, 2185–2208.

30. Fuka, D.R.; Walter, M.T.; MacAlister, C.; Degaetano, A.T.; Steenhuis, T.S.; Easton, Z.M. Using the Climate Forecast System Reanalysis as weather input data for watershed models. *Hydrol. Process.* **2014**, *28*, 5613–5623.

31. Tarboton, D. TauDEM. Available online: https://hydrology.usu.edu/taudem/taudem5/downloads.html (accessed on 15 May 2021).

32. Jenkinson, A. The frequency distribution of the annual maximum (or minimum) values of meteorological events. *QJ Roy. Meteor. Soc.* **1955**, *87*, 158–171.

33. OriginPro, V. *OriginLab Corporation*; OriginLab Corporation indicates: Northampton, MA, USA; 2016.

34. Soil Conservation Service. *National Engineering Handbook, Section 4, Hydrology*; Soil Conservation Service: Washington, DC, USA, 1972; pp. 1–20.

35. Monteith, J. Evaporation and the environment. *Jawra J. Am. Water Resour. Assoc.* **1965**, *19*, 205–234.

36. Venetis, C. A study on the recession of unconfined acquifers. *Int. Assoc. Sci. Hydrology. Bull.* **1969**, *14*, 119–125.

37. Williams, J. Sediment routing for agricultural watersheds 1. *JAWRA J. Am. Water Resour. Assoc.* **1975**, *11*, 965–974.

38. Williams, J. Chapter 25: The EPIC model. *Comput. Model. Watershed Hydrol.* **1995**, 909–1000.

39. Bagnold, R. Bed load transport by natural rivers. *Water Resour. Res.* **1977**, *13*, 303–312.

40. Dell'Oca, A.; Riva, M.; Guadagnini, A. Moment-based metrics for global sensitivity analysis of hydrological systems. *Hydrol. Earth Syst. Sci.* **2017**, *21*, 6219–6234.